Rayleigh Scattering of Laser and Synchrotron Radiation from Pulsed Free Jets of Ar_n and $(N_2O)_n$ Clusters

Andrew M. Bush,[†] Andrew J. Bell,[‡] and Jeremy G. Frey*

Department of Chemistry, University of Southampton, Southampton, SO17 1BJ, U.K.

J.-M. Mestdagh

Service des Photons Atomes et Molecule, CEN-Saclay, bat 522, 91191 Gif sur Yvette Cedex, France

Received: March 13, 1998; In Final Form: May 28, 1998

Rayleigh scattering has been used to determine the average size of clusters formed in pulsed free-jet expansions of Ar and N_2O. The scaling behavior of the mean cluster size with backing pressure predicted by Hagena (*Rev. Sci. Instrum.* **1992**, *63*, 2374) and Buck and Krohne (*J. Chem. Phys.* **1996**, *105*, 5408) has been shown to be applicable up to at least an average cluster size of 25 000. A similar scaling of the average cluster size with pressure was observed for both Ar and N_2O. Competing photochemical and photophysical processes are shown to limit the use of short-wavelength radiation to observe Rayleigh scattering from the N_2O clusters.

1. Introduction

To obtain the most information from cluster experiments, the cluster size distribution is required. In the case of weakly bound van der Waals clusters, determining even the average size of neutral clusters formed in an expansion is a nontrivial task. TOF mass spectrometry has been one of the most widely used techniques in the study of cluster size and cluster size distributions. However, fragmentation of the clusters upon ionization means that the measured ion distribution may not be an accurate representation of the original neutral cluster size distribution.[1] High-energy electron diffraction is an alternative method that has been used to determine absolute cluster sizes; for example, it has been used in the case of Ar clusters in the range $20 < \bar{n} < 750$ [2] (where $\bar{n}$ refers to the average number of monomer units per cluster). Although this method can be applied directly to neutral clusters, it is relatively insensitive to cluster size.[3] Other methods include the "slow-down" method developed by Cuvellier et al.,[4] while Buck and Krohne[5] have used crossed molecular beams to measure He atoms scattered off Ar clusters. The resulting diffraction oscillations in the total differential cross section have been used to calculate the mean size of Ar clusters for $6 \leq \bar{n} \leq 90$.

Rayleigh scattering of visible radiation has been used to study the onset of nucleation in cluster beams produced by a variety of Laval nozzles.[6] Bell et al.,[7] used Rayleigh scattering as a means of determining average cluster sizes in the region $150 < \bar{n} < 4000$ for an Ar beam. Although Rayleigh scattering provides a direct approach to the measurement of cluster size and can be used over a relatively wide range of cluster sizes, absolute cluster size determination is not practical except for very large clusters where differential Rayleigh scattering cross sections can be obtained. Such cross sections have been obtained for a beam of neutral hydrogen clusters with radii larger than 1000 Å.[8]

The Rayleigh scattering signal, R, arising from the scattering of incident radiation of intensity $I(\lambda)$, at a wavelength of λ, from N spherical particles is given by

$$R = \epsilon I(\lambda) N \sigma \tag{1}$$

where ϵ is the detection efficiency that depends on the detection geometry, as well as the (wavelength dependent) response of the photomultiplier, and σ is the Rayleigh scattering cross section.

The number of scattering particles (clusters) will be proportional to the cluster flux, F_C. In the experiments of Bell et al.[7] the cluster flux was measured directly in terms of the equivalent monomer flux by breaking up the clusters and measuring the pressure in a Pitot tube. This was not possible in the present pulse-beam experiments. The average cluster flux F_C can, however, be estimated because it will be proportional to the free-jet expansion monomer flux, F_M, along the center line of the expansion:

$$F_C \propto \frac{F_M}{\langle n \rangle} \tag{2}$$

where $\langle n \rangle$ is the mean number of monomers in the cluster. The center line monomer flux, F_M, will be proportional to the total mass flow, J_0, through the nozzle. The total mass flow through the nozzle for the Ar and N_2O expansions studied here will be very similar because they have similar masses. However, the different heat capacity ratios, γ, mean that the velocity of the flow and thus the number density will be different. Expressions for the relative number density in the expansion downstream of the nozzle, N/N_0, for monatomic and diatomic gases can be found in Table 1 of ref 9.

$$N \propto \frac{yJ_0}{\langle n \rangle} \tag{3}$$

The factor y is a gas dynamic term that depends on the distance from the nozzle, the diameter of the nozzle, and the specific

[†] Current address: Lead Development Association International, 42 Weymouth Street, London, W1N 3LQ, U.K.

[‡] Current address: DERA, CBD Porton Down, Salisbury, Wilts, SP4 0JQ, U.K.

S1089-5639(98)01481-9 CCC: $15.00
Published on Web 07/18/1998

heat ratio, γ, of the gas. For a given gas the gas dynamic factor, y, will be independent of the source pressure, P_0, if the heat capacity of the gas is independent of temperature and if the flow pattern is independent of the degree of condensation. Although the former condition is true for Ar it is not strictly true for N_2O with a temperature-dependent γ. The more massive clusters will have a tendency to be concentrated in the center of the expansion, though the energy liberated on condensation to form these clusters may reheat the expansion. We assume that once conditions are produced such that large clusters are formed, the flow conditions will not vary significantly with pressure. Thus, for a given gas at a fixed source temperature with source pressure P_0,

$$N \propto \frac{J_0}{\langle n \rangle} \propto \frac{P_0}{\langle n \rangle} \tag{4}$$

For comparisons among different gases, the gas dynamic terms will be much more important (section 4.5).

Following Bell et al.[7] the Rayleigh scattering cross section, σ, for assumed spherical clusters of radius r, consisting of $\langle n \rangle$ monomers and refractive index i is given by

$$\sigma \propto \frac{r^6}{\lambda^4}\left(\frac{i^2-1}{i^2+2}\right)^2 \propto \frac{\langle n^2 \rangle}{\lambda^4}\left(\frac{i^2-1}{i^2+2}\right)^2 \tag{5}$$

For a specific gas under conditions where the source pressure is varied and the scattering signal is observed at a fixed wavelength,

$$R \propto \left(\epsilon\frac{I(\lambda)}{\lambda^4}\right)\left(\frac{i^2-1}{i^2+2}\right)^2\left(\frac{\langle n^2 \rangle}{\langle n \rangle}\right)P_0 \tag{6}$$

The first two terms in eq 6 depend on wavelength, and for an extended range of excitation wavelengths (such as used in the synchrotron experiments), the appropriate average must be calculated. If we further assume that the solid- or liquidlike nature of the clusters is independent of their size, then the refractive index of the clusters will also not depend on their size. Therefore,

$$R \propto \frac{\langle n^2 \rangle}{\langle n \rangle}P_0 \tag{7}$$

Small, perhaps liquid-like, clusters may have a different refractive index, but once conditions are met such that larger, solid-like clusters are formed, the assumption of a constant refractive index should be reasonable. The influence of the refractive index will be considered in more detail for Ar and N_2O in sections 4.2, 4.3, and 4.5.

If the cluster distribution is not too broad so that

$$\langle n^2 \rangle \cong \langle n \rangle^2 \tag{8}$$

$$\bar{n} = \langle n^2 \rangle / \langle n \rangle \tag{9}$$

then the effective mean cluster size will be designated by $\bar{n}$.

$$R \propto \bar{n}P_0 \tag{10}$$

$$\bar{n} \propto R/P_0 \tag{11}$$

Thus, the observation of a nonlinear dependence of the Rayleigh signal as a function of expansion pressure reveals the changes in the relative average cluster size.

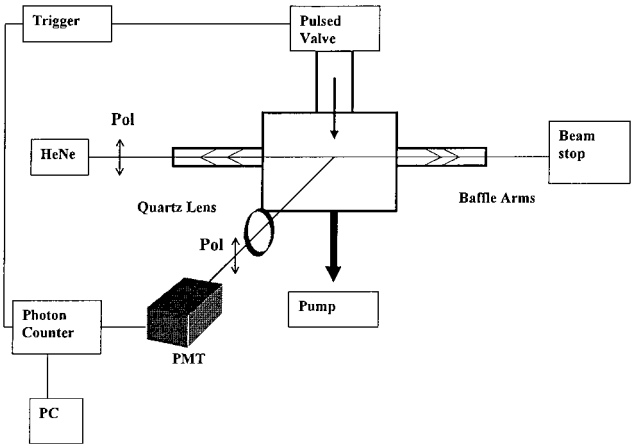

Figure 1. Schematic of the experimental apparatus used to observe scattering with a HeNe laser.

The primary aim of the work presented was to assess the practicality of using Rayleigh scattering as a method of cluster size determination in pulsed free-jet beams and to assess the usefulness of shorter wavelengths in extending the range of clusters sizes that can be probed.

2. Experimental Section

The diagram of the apparatus used in these investigations is shown in Figure 1. A pulsed valve (General Valve, 500 μm orifice, 10 Hz repetition rate) was used and operated with a Teflon or polypropylene poppet with backing pressures behind the nozzle up to 25 bar. It produced a pulse width of typically 600 μs. The vacuum chamber base pressure of approximately 1×10^{-6} mbar was maintained using a single diffusion pump (Edwards E09K, 9 in. diameter backed by a two-stage rotary pump, Alcatel 1012A) rising to ca. 1×10^{-3} mbar at the highest nozzle pressures. The free-jet expansion was directed straight into the diffusion pump, maximizing the efficiency of pumping and reducing scattered gas to a minimum.

Relative flux measurements on the expansion were made using an ion gauge (Edwards IG40K head and Ion 8 controller) connected to a digital oscilloscope (Gould 4062). These measurements were made by placing an aluminum deflection plate (approximately 15 cm $\times$ 15 cm) in the path of the expansion at an angle of 45° to the jet. This plate was used to deflect the jet toward an ion gauge head placed at the rear of the vacuum chamber. The resulting dispersion of the jet avoided saturation of the ion gauge, which was observed if the ion gauge was placed directly in the gas pulse.

The collimated output from an unpolarized HeNe laser (Melles Griot, 543.5 nm, 4 mW) was polarized and entered the vacuum chamber through a Brewster angled window and a 1 m baffle arm. The inside of the vacuum chamber was coated black to minimize background scattered light. Within the chamber the laser beam crosses the expansion perpendicularly at 2.0 cm from the nozzle orifice. This distance gave the optimum S/N ratio for the Rayleigh scattered signal from a high-pressure N_2O beam. The laser beam leaves the chamber through a second baffle arm sealed by a Brewster angled window fitted with a Woods horn. The Rayleigh scattered radiation was collected by a quartz lens with the axis mutually perpendicular to the laser beam and the jet, and it was focused through a second vertical plane polarizer and aperture onto a photomultiplier tube (PMT, Thorn EMI 9924QB). The aperture restricted the region imaged to a diameter of ca. 2 mm. The output from the PMT was amplified by a fast preamplifier (Ortec 9301) and

recorded using a gated photon counter (Stanford Research Systems SRS500) with the gate set to cover the gas pulse. When the temporal profile of the scattered signal was recorded, a multichannel scaler (EG&G Ortec, ACE gate width of 10 μs) was used.

The synchrotron studies were carried out at the Daresbury Synchrotron Radiation Source (SRS) using a 1 m Seya-Namioka monochromator (beam line 3.1). A similar experimental arrangement was used as for the HeNe experiments. The pulsed nozzle and detection optics were orientated to allow detection of the scattering of the predominantly horizontally polarized synchrotron radiation. The monochromator was isolated from the vacuum chamber by two LiF windows with the intervening region evacuated by a turbopump. An aperture was used to produce a rectangular illumination (ca. 10 $\times$ 2 mm) of the expansion. The distance between the nozzle and the interaction region was optimized at 4.0 cm to give the maximum signal-to-noise ratio for a beam of N_2O. This was further from the nozzle than in the comparable laser experiments, since the larger synchrotron beam led to increased scattering from the nozzle at shorter nozzle-beam distances.

Preliminary experiments indicated that the monochromator throughput, even with the slits fully open, was insufficient to give a detectable scattered signal; all experiments reported here were therefore carried out with the monochromator at zero order. The LiF windows mean that without further filters, radiation in the region 120−1000 nm entered the vacuum chamber. Some additional wavelength discrimination was obtained by placing optical filters in the path of the synchrotron beam, in front of the PMT detector, or both.

3. Results

3.1. Molecular Beam Flux Measurements. The response time of the ion gauge monitoring the deflected beam was not fast enough to measure accurate temporal profiles. For both Ar and N_2O the integrated area of the ion gauge signal recorded as a function of time was found to be directly proportional to the applied pressure, confirming the linear relationship between the total flux of atoms or molecules in the expansion and the nozzle pressure, P_0.

3.2. Scattering Results for Ar. Figure 2a shows the scattered signal detected as a function of P_0 for expansions of Ar up to 25 bar using 543.5 nm HeNe radiation and synchrotron radiation (zero-order monochromator, LiF window, and no filters). The observed pressure dependence is similar in the two experiments. For the HeNe experiment each point was obtained by summing 1200 gas pulses. In comparison 5000 pulses were used with the synchrotron source.

The time-resolved scattering profiles shown in Figure 2b change slightly with pressure and do not have the ideal "flat" top profile. This is most likely due to incomplete opening of the pulsed valve. Calculations on the time needed to accelerate the Ar following the opening of the valve[10] indicate that even at the highest pressures (25 bar) this will only take about 40 μs. Steady-state conditions will then be established, and the expansion will smoothly follow changes in the effective nozzle pressure. Comparison of the Rayleigh scattering intensity as a function of pressure from different sections through the pulse suggests that the pressure is about 20% lower at the start and end of the pulse than it is through the central part of the pulse. The observed Rayleigh signal is dominated by this central part of the gas pulse.

3.3. Results for N_2O. Figure 3a shows the pressure dependence of the scattered signal from N_2O beams up to 25 bar using the HeNe laser (summing over 1200 gas pulses for each pressure). The time-resolved scattering pulse profiles were similar to those observed for Ar. With the synchrotron monochromator at zero order and with detection at all wavelengths (excitation at ca. 120−1000 nm, detection at ca. 200−700 nm), a *linear* dependence on stagnation pressure is observed for the scattered light (Figure 3b). However, a *nonlinear* increase in scattered signal with P_0 is observed (the data points in Figure 3c) from a similar experiment performed with a WG335 colored filter placed in front of the PMT, i.e., detecting light from wavelengths in the region of ca. 335−700 nm. Figure 3c shows the very good agreement between results from the HeNe laser (solid line, scaled fit from Figure 3a) and the filtered synchrotron experiment.

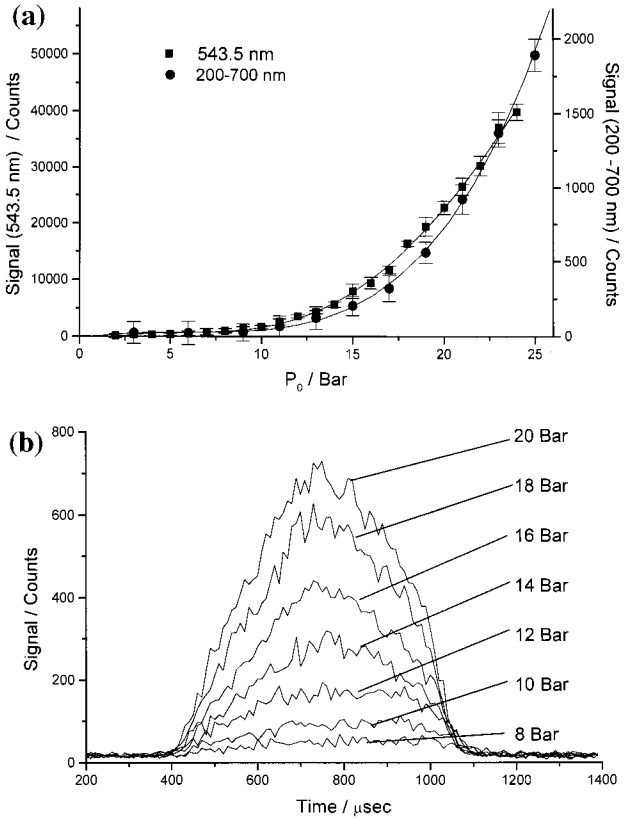

Figure 2. Rayleigh scattered signal vs P_0 for the Ar free-jet expansion (a) recorded using a 543.5 nm HeNe laser (left *y* axis) and the synchrotron source detecting 200−700 nm (right *y* axis) and (b) temporal profiles recorded with 543.5 nm HeNe laser (10 μs intervals).

Figure 4 (solid squares) shows the detected light signal observed for N_2O at $P_0 = 14$ bar using different filters with synchrotron radiation. The data shown were obtained by integrating the pulse profiles obtained for each of the arrangement of filters. All synchrotron results have been corrected for variations in photon flux due to changes in the synchrotron storage ring current. The results show that in the synchrotron experiments approximately 60% of the scattered signal shown in Figure 3b derives from wavelengths below 280 nm. The calculated points (Figure 4 circles) show the expected signal intensity assuming only contributions from Rayleigh scattering. The calculation will be described in more detail in section 4.4.

4. Discussion

4.1. Scaling Laws. The average cluster sizes inferred from the Rayleigh scattering will be discussed in the context of the scaling behavior with the expansion stagnation pressures. The reduced scaling factor Γ^*, introduced by Hagena,[9,11,12] depends

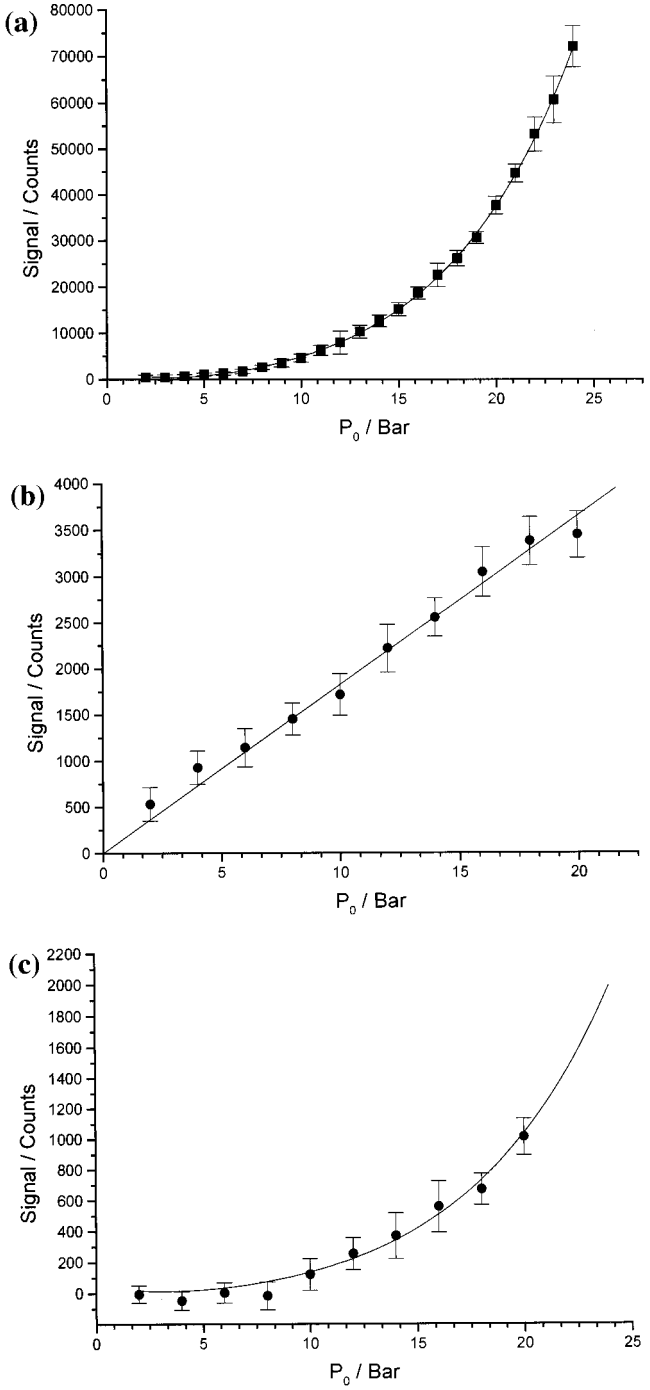

Figure 3. Rayleigh scattered signal vs P_0 for the N_2O free-jet expansion for total scattered photon counts from (a) a 543.5 nm HeNe laser, (b) the synchrotron source detecting 200−700 nm, and (c) the synchrotron source with a WG335 filter in front of the PMT detecting 335−700 nm. The solid curve is a scaled version of the HeNe data in part a.

on the characteristics of the expansion gas (density of the solid, enthalpy of sublimation) and the expansion conditions. For an Ar expansion through a sonic nozzle (diameter d) the scaling factor Γ* is given by (from eq 7 of ref 5)

$$\Gamma^* = 1646(P_0/\text{mbar})(d/\mu\text{m})^{0.85}(T_0/K)^{-2.2875} \qquad (12)$$

For a fixed nozzle diameter and temperature, Γ* will be proportional to P_0. Hagena has related Γ* to the mean cluster size of Ar atoms using results obtained from mass spectrometry.[12,14] For $1000 < \Gamma^* < 7300$,

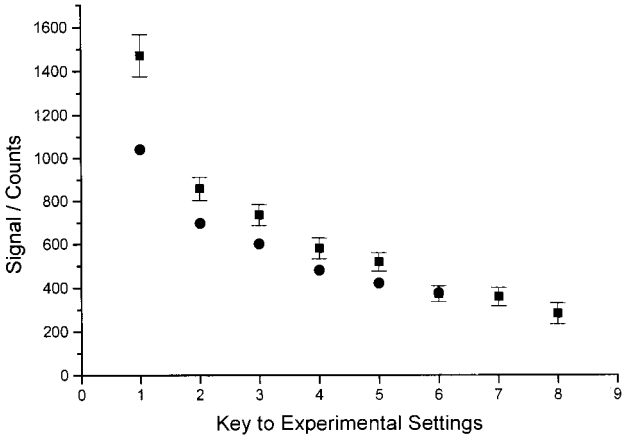

Point	Incident Wavelength Range	Detected Wavelength Range
1	120-1000 nm	200-700 nm
2	120-1000 nm	280-700 nm
3	120-1000 nm	295-700 nm
4	120-1000 nm	305-700 nm
5	120-1000 nm	320-700 nm
6	120-1000 nm	335-700 nm
7	335-700 nm	200-700 nm
8	335-700 nm	320-700 nm

Figure 4. Detected counts from a 14 bar N_2O expansion (■) using synchrotron radiation. The filters used were for wavelength ranges depicted in the figure. The calculations giving the circles (●) are described in section 4.4.

$$\bar{n} = 33(\Gamma^*/1000)^{2.35} \qquad (13)$$

Buck and Krohne[5] have reported a second relationship between Γ* and mean cluster size for $350 \le \Gamma^* \le 1800$:

$$\bar{n} = 38.4(\Gamma^*/1000)^{1.64} \qquad (14)$$

They recommend the use of eq 13 for $\Gamma^* \ge 1800$. From eq 12 with $T_0 = 300$ K and $d = 500$ μm, the "break point", $\Gamma^* = 1800$, corresponds to $P_0 = 2.55$ bar at the lower end of the experiments reported here, and eq 14 then gives $\bar{n} = 101$. At 24 bar, the highest pressure used, $\Gamma^* = 17\,000$ and $\bar{n}$ is ca. 26 000 from eq 13. The results of Hagena and Buck and Krohne have shown that eq 13 is applicable over the range $90 \le \bar{n} \le 10\,000$. The upper limit of 10 000 atoms per cluster was set by the fact that no experimental data had been reported for $\bar{n} > 10\,000$.

4.2. Ar Clusters. The derivation of the Rayleigh scattering signal, section 2, assumed that the refractive index of the cluster was independent of the cluster size. The electron diffraction studies of Farge et al.[2] suggest that for $20 < \bar{n} < 50$ the clusters have a noncrystalline polyicosahedral structure but for $50 < \bar{n} < 750$ the structure consists of multiple layers of icosahedra. For larger clusters the diffraction patterns were interpreted in terms of a bulk fcc crystalline structure, but work by van der Waal suggests that there is no evidence for a transition to an fcc structure.[15] The structural work implies that the solid-phase refractive index would be most appropriate for the clusters. Even the small difference between the refractive index for liquid Ar, 1.226, and solid Ar, 1.265 (derived from the dielectric constant[16] because dispersion will not be significant in the visible), would make ca. a 40% change in the Rayleigh scattering intensity.

The results presented in Figure 2 do not show any sign of a discontinuity corresponding to a change in phase, and so it is reasonable to assume that the Rayleigh signal is proportional

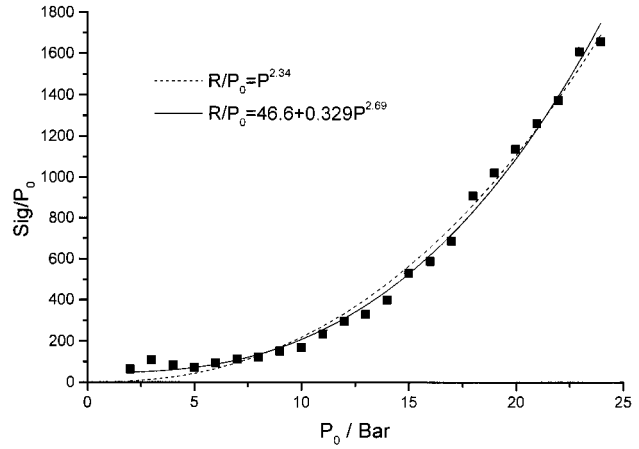

Figure 5. R/P_0 vs P_0 from the Rayleigh scattering results of an Ar jet with the HeNe laser. The dashed line is a least-squares fit to a power law giving a $P_0^{2.34}$ dependence. The solid line is a fit including a constant term with a $P_0^{2.69}$ dependence.

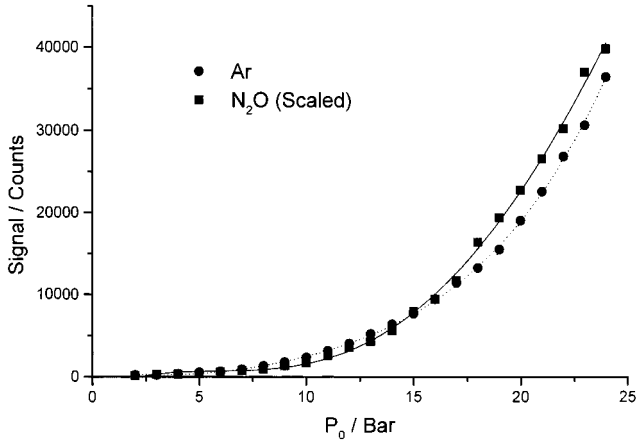

Figure 6. Scattering of HeNe 534.5 nm radiation vs P_0 for expansions of Ar (●) and N_2O (■). The latter scaled by a factor of 0.5.

to the average cluster size and the nozzle pressure. The nonlinear increase in the Rayleigh scattering signal with P_0 over the range 2−25 bar, Figure 2a, can then only result from an increase in the value of $\bar{n}$ as the pressure is increased. Because absolute cluster size cannot be determined from the Rayleigh scattering data presented here, it is not possible to confirm that the scaling equations correctly predict the average Ar cluster size in this experiment. However, the scaling laws predict a power law dependence of the form

$$R/P_0 \propto \bar{n} \propto \Gamma^{2.35} \propto P_0^{2.35} \qquad (15)$$

Figure 5 shows a plot of (R/P_0) vs P_0. A least-squares fit to a power law (dashed line) gives a $P_0^{2.36}$ dependence, which agrees well with the predicted scaling law pressure dependence for $P_0 > 5$ bar. A slightly better fit is obtained when a constant term is included; a higher power index of 2.69 is then obtained. The relatively small constant term may correspond to scattering from uncomplexed monomers. The agreement between experiment and the scaling relationship is maintained above 16 bar, the limit of previous investigations (corresponding to clusters containing more than 10 000 Ar atoms). This suggests that the scaling law is applicable for the formation of clusters containing up to 25 000 Ar atoms.

4.3. N_2O Clusters. The similarity of the P_0 dependence of the scattering of HeNe light by Ar and N_2O, Figure 6, indicates that Rayleigh scattering is responsible for the signal observed from the N_2O clusters. The similar response of scattered signal with P_0 for the HeNe laser and the filtered synchrotron experiments, Figure 3c, shows that the scattering observed above 335 nm is also the result of Rayleigh scattering. A power law provides a good fit to the HeNe scattering data, Figure 3a, with $R \propto P_0^{3.52}$, thus,

$$\bar{n} \propto R/P_0 \propto P_0^{2.52}$$

suggesting a slightly higher order dependence of the average cluster size on pressure for N_2O than for Ar.

Spectroscopic studies of N_2O clusters point to the onset of solidlike behavior for $\bar{n} > 35$,[17] although the FTIR studies of Gauthier[18] suggest that the structure of these clusters is neither that of the liquid or solid. At 300 K the refractive index of liquid N_2O is about 1.26, but it increases sharply with pressure and near the melting point has a value of about 1.43.[19] The high-frequency limit of the dielectric constant of solid N_2O at 162 K gives a similar value for the refractive index of 1.409.[20] The increase in the refractive index from the liquid to solid value would correspond to an increase in the Rayleigh scattering intensity by a factor of about 2. The smooth dependence of the Rayleigh scattering on pressure provides no indication of a phase transition for the range of cluster sizes studied.

4.4. Wavelength Dependence. The wavelength resolution available using the filters in conjunction with the synchrotron is coarse, and comparison among different filters requires averaging over the wavelength-dependent terms. The Rayleigh scattered signal depends on the wavelength dependence of the synchrotron photon flux, the PMT detection efficiency, filter transmission, the cluster refractive index, and the λ^{-4} dependence of Rayleigh scattering. These terms were modeled over the response region of the PMT (200−700 nm).

The PMT detector response and filter transmission are known from manufacturers' specifications. Direct experimental measurement of zero-order photon flux was not possible in these experiments. The photon flux was calculated on the basis of the diffraction efficiencies of a perfectly coated diffraction grating.[21] However, contamination of the grating surface can significantly modify diffraction efficiencies, and "ideal" diffraction efficiencies and derived fluxes must be treated with caution.

The wavelength dependence of the refractive index was taken from the work of Zeiss and Meath[22] who have used calculated dipole oscillator strength distributions to evaluate the gas-phase refractivity, $i_R(\lambda)$, of N_2O as a function of wavelength in the visible and ultraviolet regions of the spectrum. The refractivity increases significantly at short wavelengths because of the proximity of N_2O absorption bands.[23−26] The wavelength dependence of the solid-phase refractive index was obtained by scaling the gas-phase data to match the refractive index in the visible region.[20] It is possible that there could be some quantum effects associated with the excitations in the small clusters, changing the energy levels in a manner akin to quantum dots. This would not influence the refractive index at the HeNe wavelength but might make a contribution at shorter wavelengths near the N_2O absorption features. A wavelength resolved study would be required to elucidate any such effects.

The similarity of the HeNe results and the synchrotron data above 335 nm suggests that the scattered light detected when either the incident or detected light is restricted to be longer than 335 nm (Figure 4, points 6 and 8) results from pure Rayleigh scattering. By adjustment of the wavelength-dependent terms, the Rayleigh signal can calculated for the 120−1000 nm incident synchrotron radiation and scaled to the results for

$\lambda > 335$ nm. Figure 4 shows that the experimental scattering levels are significantly higher than the calculated Rayleigh scattered signal in the short-wavelength region, suggesting that a second process is responsible for a significant proportion of the observed signal, with the proportion increasing to lower wavelengths. A comparison of the different filter arrangements shows that the majority of the "excess" radiation must be at wavelengths shorter than 335 nm. This additional process, dominating the observed signal below 335 nm, could account for the linear increase in detected radiation with pressure (Figure 2b).

Comparison of the scattering in the regions 200−700 nm (Figure 2b) and 335−700 nm (Figure 2c) shows that even at low pressures where little Rayleigh scattering is expected, there is still a significant signal when the beam is irradiated with the short-wavelength radiation. This, coupled with the linear rise in the signal with pressure, suggests that a process linear in the N_2O flux is contributing to most of the observed signal. This may arise from excitation of N_2O below 200 nm, resulting in fluorescence above 300 nm. Sponer and Bonner[23] have reported a very weak optical absorbance for N_2O in the region 260−310 nm. More intense absorption bands have been observed in the regions 160−250 nm,[24−26] 138−159 nm,[24,26] and 118−138 nm,[24,26] corresponding to transitions from the $X^1\Sigma^+$ state to the $B^1\Delta$, $C^2\Pi$, and $D^1\Sigma^+$ N_2O states, respectively.[27]

The photodissociation of N_2O between 185 and 230 nm[28] produces mainly ground-state nitrogen molecules and oxygen atoms predominantly in the excited $O(^1D)$ state with some $O(^1S)$. The "forbidden" transition of $O(^1D)$ down to $O(^3P)$ is unlikely to contribute directly to the observed emission. The emission from $O(^1S)$ to $O(^1D)$ at 557.7 nm could contribute to the detected signal. However, the filter experiments suggest that the excess radiation is at much shorter wavelengths (otherwise, the results of placing the WG335 filter in the synchrotron beam or before the PMT would differ).

A two-step process in which an initially formed photofragment, such as $O(^1D)$, reacts further to give electronically excited products could give rise to the observed emission The reaction of $O(^1D)$ with N_2O is known to follow two paths with almost equal probability.[29] They are

$$O(^1D) + N_2O \rightarrow 2NO \quad (16)$$

$$\rightarrow N_2 + O_2 \quad (17)$$

where the products are formed in their ground electronic states. Furthermore, two studies by Honma and co-workers[30] have indicated the formation of NO and N_2 in a supersonic expansion via the laser-initiated half reaction

$$(N_2O)_2 + h\nu\ (193\ \text{nm}) \rightarrow N_2O{\cdot}O(^1D) + N_2 \rightarrow 2NO + N_2 \quad (18)$$

In this experiment, fluorescence was detected as a result of $NO(D^2\Sigma^+, v = 1) \leftarrow NO(X^2\Pi, v = 2)$ excitation, which also occurs at 193 nm. There is the possibility that similar processes occur in the synchrotron experiments reported in this work, and irradiation using a broad band of wavelengths, e.g., 110−335 nm, allows excitation and fluorescence from many more states of NO, N_2, and O_2. However, dissociation followed by excitation and fluorescence is a two (or more) photon process and the relatively low intensity of the synchrotron radiation used may mean that such mechanisms have low overall probability.

A small fraction of the N_2O may dissociate to give $N(^2D)$ that can react to give excited NO, which could provide the required emission with a single-photon excitation, i.e.,

$$N(^2D) + N_2O \rightarrow NO(B^2\Pi) + N_2 \quad (19)$$

4.5. Comparison of the Rayleigh Scattering from Ar and N_2O. A comparison of the scattering from Ar and N_2O clusters is shown in Figure 6. They follow a similar form with the scattering being about twice as intense for N_2O. If the clusters are liquidlike, then the refractive index terms in the Rayleigh scattering eq 6 will be similar (refractive index for Ar and N_2O are 1.226 and 1.26, respectively; see sections 4.2 and 4.3). If, however, the clusters are solidlike, then the difference in refractive index (1.26 and 1.4 for Ar and N_2O, respectively) means that for equal numbers of the same-sized clusters, the N_2O clusters will scatter about twice as much as comparable Ar clusters. The total mass flow from the nozzle will be very similar for Ar and N_2O. However, the center line density downstream of the nozzle would be expected to be significantly different because of the different properties of the expansions of monatomic and polyatomic gases; see the gas dynamic term referred to in section 2. Even if N_2O could be considered effectively as a diatomic, the beam density would be about half that of the Ar beam.[9] Thus, N_2O clustering must be at least twice as effective as for Ar for the same P_0.

In a series of experiments Hagena compared expansions of CO_2 with those of Ar and N_2[9,14] under similar conditions. The clustering behavior of CO_2 was closer to that of Ar than to that of N_2 e.g., $\bar{n} = 1000$ at pressures of 3×10^3, 2×10^3, and 10^4 Torr for Ar, CO_2, and N_2, respectively, at 298 K. The CO_2 results show a higher order pressure dependence than Ar results (but less than N_2 results). Figure 6 shows that this is also the case for the N_2O data recorded here by Rayleigh scattering. As yet, there are no theoretical scaling laws for comparison.

5. Conclusions

Rayleigh light scattering has been used successfully to determine the presence and relative size of both Ar and N_2O clusters produced in a pulsed free-jet expansion. These experiments were performed using HeNe laser radiation at 543.5 nm and synchrotron radiation from 200 to 700 nm. By use of results obtained with HeNe radiation, the pressure dependence of the average Ar cluster size was compared to the scaling law equations for Ar proposed by Hagena[12] and Buck and Krohne.[5] Agreement with the scaling laws was found to be good within the previously suggested limits of $1800 \leq \Gamma^* \leq 11\,500$, where Γ^* is the reduced parameter of Hagena.[11] Furthermore, agreement with the scaling laws was shown to extend to the cluster size limit of the experimental apparatus, corresponding to $\Gamma^* \approx 17\,000$. Pressure-dependent results obtained for N_2O using HeNe radiation show a trend similar to the trend from the Ar results, although at the present time scaling laws are not available for comparison.

By use of synchrotron radiation, the pressure dependence of scattering from an Ar beam has been observed over the region 200−700 nm. For N_2O, results were obtained by detecting over the wavelength regions 335−700 and 200−335 nm. The scattered signal from Ar clusters, and also from N_2O clusters in the region 335−700 nm, shows the same nonlinear pressure dependence as in the respective HeNe experiments. The linearly pressure-dependent scattered signal from N_2O over the range 200−335 nm was attributed to fluorescence originating from chemiluminescence of a photolysis product of N_2O.

Acknowledgment. We thank the EPSRC, Royal Society and the British Council for financial support and the Daresbury staff, particularly C. S. Mythen for their help in the use of the SRS.

References and Notes

(1) Buck, U. *J. Phys. Chem.* **1988**, *92*, 1023 and references therein.
(2) Farges, J.; de Feraudy, F.; Raoult, B.; Torchet, G. *J. Chem. Phys.* **1983**, *78*, 5067; *J. Chem. Phys.* **1986**, *84*, 3491.
(3) Kappes, M.; Leutwyler, S. *Atomic and Molecular Beam Methods*; Scoles, G., Bassi, D., Buck, U., Laine, D., Eds.; Oxford University Press: Oxford, U.K., 1988; Vol. 1, p 398.
(4) Cuvellier, J.; Meynadier, P.; de Pujo, P.; Sublemontier, O.; Visticot, J.-P.; Berlande, J.; Lallement, A.; Mestdagh. J. M. *Z. Phys. D* **1991**, *21*, 265.
(5) Buck, U.; Krohne, R. *J. Chem. Phys.* **1996**, *105*, 5408.
(6) Abraham, O.; Kim, S.-S.; Stein, G. *J. Chem. Phys.* **1981**, *75*, 402.
(7) Bell, A. J.; Mestdagh, J. M.; Berlande, J.; Biquard, X.; Cuvellier, J.; Lallement, A.; Meynadier, P.; Sublemontier, O.; Visticot, J.-P. *J. Phys. D* **1993**, *26*, 994.
(8) Klingerhöfer, R.; Moser, H. O. *J. Appl. Phys.* **1972**, *43*, 4575.
(9) Hagena, O. F. *Surf. Sci.* **1981**, *106*, 101.
(10) Saenger, K. L. *J. Chem. Phys.* **1981**, *75*, 2467.
(11) Hagena, O. F. *Z. Phys. D* **1987**, *4*, 291.
(12) Hagena, O. F. *Rev. Sci. Instrum.* **1992**, *63*, 2374. Hagena, O. F. *Phys. Fluids* **1974**, *17*, 894.
(13) Wormer, J.; Guzielski, V.; Stapelfeldt, J.; Moller, T. *Chem. Phys. Lett.* **1989**, *159*, 321.
(14) Hagena, O. F.; Obert, W. *J. Chem. Phys.* **1972**, *56*, 1793.
(15) van der Waal, B. *Phys. Rev. Lett.* **1996**, *76*, 1083.
(16) Amey, R. L.; Cole, R. H. *J. Chem. Phys.* **1964**, *40*, 146.
(17) Miller, R. E.; Watts, R. O.; Ding, A. *Chem. Phys. Lett.* **1984**, *83*, 155.
(18) Gauthier, M. *J. Chem. Phys.* **1988**, *88*, 5439.
(19) Shimizu, H.; Sakoh, H.; Sasaki, S. *J. Phys. Chem.* **1994**, *98*, 670.
(20) Nary, K. R.; Kuhns, P. L.; Conradi, M. S. *Phys. Rev. B* **1982**, *26*, 3370.
(21) Mythen, C. S. Daresbury Laboratory, private communication, 1995.
(22) Zeiss, G. D.; Meath, W. J. *Mol. Phys.* **1977**, *33*, 1155.
(23) Sponer, H.; Bonner, L. G. *J. Chem. Phys.* **1940**, *8*, 33.
(24) Zelikoff, M.; Watanabe, K.; Inn, E. C. Y. *J. Chem. Phys.* **1953**, *21*, 1643.
(25) Bates, D. R.; Hayes, P. B. *Planet. Space Sci.* **1967**, *15*, 189. Johnston, H. S.; Selwyn, G. S. *Geophys. Res. Lett.* **1975**, *2*, 549.
(26) Rabalais, J. W.; McDonald, J. M.; Scherr, V.; McGlynn, S. P. *Chem. Rev.* **1971**, *71*, 73.
(27) Hopper, D. G. *J. Chem. Phys.* **1984**, *80*, 4290.
(28) Chamberlain, G. A.; Simons, J. P. *J. Chem. Soc., Faraday Trans. 2* **1975**, *71*, 402. Zavelovich, J.; Rothschild, M.; Gornik, W.; Rhodes, C. K. *J. Chem. Phys*. **1981**, *74*, 6787. Shafer, N.; Tonokura, K.; Matsumi, Y.; Tasaki, S.; Kawasaki, M. *J. Chem. Phys.* **1991**, *95*, 6216. Hanisco, T.; Kummel, A. *J. Phys. Chem.* **1993**, *97*, 7242.
(29) Davidson, J. A.; Howard, C, J.; Sciff, H. I.; Fahsenfeld, F. C. *J. Chem. Phys.* **1979**, *70*, 1697. Volltrauer, H. N.; Felder, W.; Pirkle, R. J.; Fontijn, A. *J. Photochem.* **1979**, *11*, 173. Marx, W.; Bahe, F.; Schurath, U. *Ber. Bunsen-Ges. Phys. Chem.* **1979**, *83*, 225.
(30) Honma, K.; Kajimoto, O. *Chem. Phys. Lett.* **1985**, *117*, 123. Honma, K.; Fujimura, Y.; Kajimoto, O. *J. Chem. Phys.* **1988**, *88*, 4739.